RSC Advances

ROYAL SOCIETY OF CHEMISTRY

www.rsc.org/advances

A facile hydrothermal method to synthesize $Sb_2S_3/Sb_4O_5Cl_2$ composite with three-dimensional spherical structure

Qian Jiang [a, b], Xingzhong Yuan [a, b *], Hou Wang [a, b], Xiaohong Chen [c], Shansi Gu [a, b], Yang Liu [a, b], Zhibin Wu [a, b], Guangming Zeng [a, b]

[a] College of Environmental Science and Engineering, Hunan University, Changsha 410082, PR China

[b] Key Laboratory of Environment Biology and Pollution Control, Hunan University, Ministry of Education, Changsha 410082, PR China

[c] Collaborative Innovation Center of Resource-Conserving & Environment-Friendly Society and Ecological Civilization, Changsha 410083, PR China

[*] Corresponding author at: College of Environmental Science and Engineering, Hunan University, Changsha 410082, PR China. Tel.: +86 731 88821413; fax: +86 731 88823701.
E-mail address: yxz@hnu.edu.cn (X.Z. Yuan)

Abstract

Three-dimensional spherical $Sb_2S_3/Sb_4O_5Cl_2$ microcrystallines were firstly synthesized via a facile hydrothermal process without any oxychlorides at 100 °C. The powder X-ray diffraction pattern showed the product corresponded to the $Sb_2S_3/Sb_4O_5Cl_2$ composites, the successful combination of the product was further confirmed by X-ray Photoelectron Spectroscopy (XPS), energy dispersive X-ray (EDX) and High-resolution transmission electron microscopic (HRTEM). Scanning electron microscopy (SEM) studies revealed that the irregular shaped nanoblocks self-organized into spherical assemblies. The suitable temperature, the possible mechanistic pathway in the formation of the structures and the mechanisms were discussed. Moreover, the as-prepared materials also had an excellent visible light photoactivity for methyl orange (MO) degradation, which could remove 82.9% MO in 60 min.

Keywords

Three-dimensional; spherical; Sb_2S_3; $Sb_4O_5Cl_2$

1. Introduction

Over the past several years, due to the controllable size, various type of unique morphology and shaped-dependent properties, three-dimensional structure materials synthesized by large-scale self-assembly of micro- and nanostructured building components have become a hot topic of material preparation.[1-8] With one-dimensional (1D) structure-based materials as building units, a variety of self-assembling morphologies such as dandelion-like[9], flower-like[10-12], urchin-like[13], peanut-like structures[14] and tube-like structures[15] have been reported. Most of these studies usually rely on spherical superstructures prepared with hydrothermal or solvothermal root[9-12]. However, due to the high temperature and surfactants, severe preparation is of high production cost for the oriented growth of building units requirements. As a result, the development of mild and surfactant-free methods for preparing three-dimensional spherical structure materials is necessary but remains a challenge.

The semiconductor composites synthesized by metal different compounds (such as ZnO/ZnS, SnS_2/SnO_2, CuO/CuS, BiOCl/BiOBr and Bi_2S_3/BiOCl) have been another hotspot in material preparation in the recent years for its outstanding physicochemical property[16-19]. For example, Lu *et al*. used a thermal evaporation process to synthesize ZnO/ZnS nanowire arrays which could be applied in electricity generation from mechanical energy[20]. Zhang and co-workers successfully prepared SnS_2/SnO_2 nanoheterojunctions via a simple one-step hydrothermal method, and photocatalytic efficiencies of the composites was higher than pure SnO_2 and SnS_2 nanoflakes at different dosages of photocatalysts[21]. In addition, Bi_2S_3/BiOCl hybrid

architectures with good visible light photocatalytic activity were also reported[22]. Friendly, antimony trisulfide (Sb_2S_3), another kind of semiconductor materials, possesses high thermoelectric power and good photosensitivity[23]. Owing to its suitable band gap (1.5-2.2 eV[24]) and wide solar spectrum, Sb_2S_3 has received significant attention for potential applications in solar energy conversion and optoelectronic material[25-30]. Sb_2S_3-based composites such as TiO_2/Sb_2S_3[25] and Ag/Sb_2S_3[31] have been widely applied to synthesize various optical materials in the application of energy and environmental field. Nevertheless, so far very few researches are focusing on the development in synthesis of the composites composed of Sb_2S_3 and antimony-based compounds.

Herein, a simple, mild and environmental (without any oxychlorides) hydrothermal method, based on the reactions of antimony trichloride and different dosages of sodium sulfide in water at 100 ˚C for 12 h, is employed for the synthesis of $Sb_2S_3/Sb_4O_5Cl_2$ microspheres with building units of one-dimensional nanostructure-based blocks and rods. Indeed, $Sb_4O_5Cl_2$ with a wide band gap of about 3.25 eV (the obtained result in this study) have matched band potentials with Sb_2S_3. What's more, it's easily to combine Sb_2S_3 with $Sb_4O_5Cl_2$ since both of them are prepared in acidic environment. Technically, this is the first time that $Sb_2S_3/Sb_4O_5Cl_2$ composites are successfully synthesized. As an example of application, the prepared samples as photocatalyst for the degradation of methyl orange (MO) are also simply discussed.

2. Experimental

For the sample preparation, characterization and Photocatalytic Activity Measurements have been shown in the Experimental section in the Supporting Information. Moreover, the molar ratio of $SbCl_3/Na_2S$ was set to be 2:3, 1:1 and 2:1, the corresponding products were denoted as C1, C2, and C3, respectively.

3. Results and discussion

3.1 Characterization of the as-obtained samples

The purity and crystallinity of the as-prepared samples are confirmed by XRD technique. Fig. 1a shows the XRD patterns of pure $Sb_4O_5Cl_2$, all the reflections of sample crystals obtained are indexed to the structure of $Sb_4O_5Cl_2$ (JCPDS Files, No.30-0091). The XRD patterns of C1, C2 and C3 samples are also shown in Fig. 1a. All the diffraction peaks of $Sb_4O_5Cl_2$ are presented in the three samples. In addition, the main diffraction peaks of Sb_2S_3 (JCPDS Files, NO.42-1393) are clearly found at 15.7° (020), 17.5° (120) and 32.3° (221). Remarkably, the XRD patterns of C1 samples show an interesting problem: the molar ratio of $SbCl_3/Na_2S$ is set to be 2:3, but the as-prepared sample is not the pure Sb_2S_3. Then the experiment is carried out with adding an excess of Na_2S, the same result is also observed. The reasons have been investigated in the following section.

Important information on the surface electronic state and composition of $Sb_2S_3/Sb_4O_5Cl_2$ are provided by XPS (Fig. S1). The survey XPS spectrum (Fig. S1a) reveals that the C2 composites are composed of Sb, O, Cl, and S, and the position of Sb 3d binding energy is superposed with that of the O 1s binding energy. Therefore,

the high-resolution XPS of Sb 3d (Fig. S1b) is taken to identify antimony chemical states. The two peaks at 529. 3 eV and 538.4 eV correspond to the Sb $3d_{5/2}$ and Sb $3d_{3/2}$, respectively, confirming the presence of Sb^{3+} cations[32]. The high-resolution spectra of S 2p shows one peak at 161.7 eV, which is consistent with the results obtained in the previous study[33]. In addition, the XPS signal of Cl 2p fitted with the peak at binding energy of 198.3 eV and 200.1 eV. On the basis of the above discussion, the $Sb_2S_3/Sb_4O_5Cl_2$ composites are successfully synthesized.

Fig. 1b and Fig. S3 show general morphologies of the as-prepared C1, C2 and C3 samples. Interestingly, the composites crystallites self-organized into spherical assemblies, and the yield of the spheres is very high. In addition, the surface of spherical particles reveals obvious edges and corners. The SEM images of pure $Sb_4O_5Cl_2$ samples are presented in Fig. 1c and Fig. S3d. These spherical morphologies are irregular and seem like a flower. It is worth noting that the structure of pure $Sb_4O_5Cl_2$ is significantly different with the composites, of which the components show different shapes and larger size (Fig. 1b and Fig. 1c). Moreover, the EDX spectrum of the C2 sample (Fig. 1d) shows the presence of Sb, O, S and Cl elements, and the molar ratio of Sb/S/Cl/O obtained from the peak area is 40.81:14.16:14.85:30.18 (the mass fraction of Sb_2S_3 is about 26.2 %), confirming the successful combination of $Sb_2S_3/Sb_4O_5Cl_2$ in the products.

In order to gain a deeper insight into the samples, HRTEM image of C2 is provided. Two kinds of lattice fringes are obviously observed in Fig. S4a. One is not well defined with an inter-layer distance (*d*-spacing) of around 0.146 nm, which

corresponds to the (431) plane for $Sb_4O_5Cl_2$. The other is ordered with a *d*-spacing of 0.363 nm, being consistent with the (101) plane of the orthorhombic structured Sb_2S_3. The elemental mapping images further verify that the hybrid microspheres are composed of Cl, O, S and Sb, and the compositional distributions of all the elements are uniform (Fig. S4b-f). These results demonstrate the heterogenous junction formation between Sb_2S_3 and $Sb_4O_5Cl_2$ architectures.

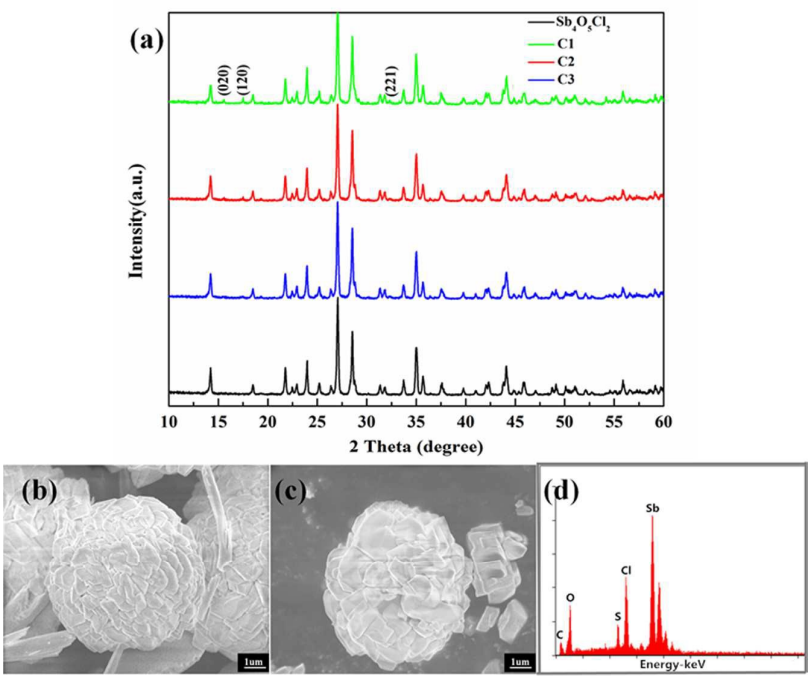

Fig.1. (a) XRD patterns of C1, C2, C3 and $Sb_4O_5Cl_2$; (b) FESEM images of C2 and (c) FESEM images of $Sb_4O_5Cl_2$; (d) The EDX spectrum of C2.

3.2 The effect factors for hybrids preparation

3.2.1 Temperatures

A temperature-dependent experiment has been conducted to explore the suitable temperature for the formation of the spherical structures of $Sb_2S_3/Sb_4O_5Cl_2$. The SEM images of $Sb_2S_3/Sb_4O_5Cl_2$ synthesized by the hydrothermal method at different

temperatures are presented in Fig. S5. Fig. S5a shows the SEM image of the obtained samples synthesized at 150°C. Compared with the samples prepared at 100°C, the spherical structure has become abnormal, and some of them are even broken. Furthermore, with an increase of the reaction temperature (200°C), it clearly shows the structure of the samples has got converted into irregular microrods with different lengths and diameters (Fig. S5b). These results indicate that the temperature plays a significant role in the synthesis of spherical structures.

3.2.2 pH

The pH value of solution also exerts an important influence on the growth of $Sb_2S_3/Sb_4O_5Cl_2$ microcrystallines. $Sb_4O_5Cl_2$ is not formed until the solution pH value is kept at 1-2[34]. On the contrary, no Sb_2S_3 deposition would be obtained for the high concentration, since they are dissolved out[5].

3.2.3 The comparison before and after hydrothermal reaction

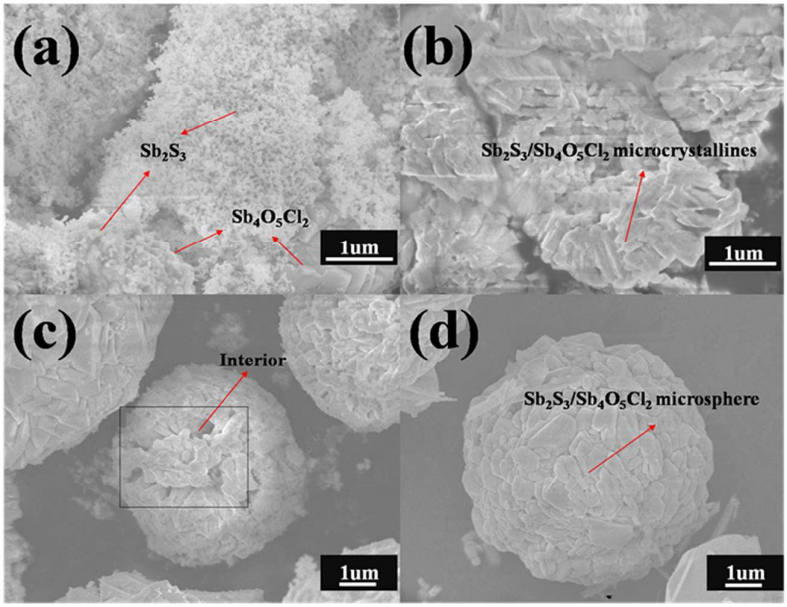

Fig.2. SEM images of the as-synthesized samples with different reaction times: (a) 0 h; (b) 4 h; (c) 8 h; (d) 12 h;

For the purpose of getting further the possible mechanism in the formation of spherical $Sb_2S_3/Sb_4O_5Cl_2$ composites, the morphology of $Sb_2S_3/Sb_4O_5Cl_2$ before and after the hydrothermal reaction is explored. The as-prepared solution turns from colorless to white when the $SbCl_3$ and HCl mixture is added into the NaOH solution. It turns out that $SbCl_3$ is strongly hydrolyzed to produce white precipitate, suggesting the formation of $Sb_4O_5Cl_2$. Then the mixture turns immediately from white to orange after the addition of Na_2S solution, demonstrating that some Sb_2S_3 are successfully obtained. After 10 minutes of stirring, the $Sb_2S_3/Sb_4O_5Cl_2$ precursors are collected and the morphology is presented in Fig. S6. Apparently, there are some scattered abnormal spheres.

Further observation shows that lots of coral-like amorphous nanoparticles have grew on the surface of irregular spheres. The irregular spheres are $Sb_4O_5Cl_2$, while the coral-like nanoparticles are Sb_2S_3, and the mechanism in the combination of $Sb_2S_3/Sb_4O_5Cl_2$ composites is an anion exchange strategy. However, before the addition of Na_2S solution, trivalent antimony ions have cooperated compactly together to form three-dimensional structures of $Sb_4O_5Cl_2$ in the process. Therefore, the S^{2-} cannot exchange for the O^{2-} and Cl^- anions, and the pure Sb_2S_3 is not able to be formed even though adding an excess of Na_2S. Moreover, after the hydrothermal reaction, the obtained regular spherical structure has been mentioned above (Fig. 1b and Fig. S3). Thus, the time-dependent experiments are developed to provide the

assembly mechanism of rule spheres. As shown in Fig. 2, for the 3h reaction time, brush-like structure generating a curvature is readily formed. The bottom of brush-like microcrystallines is composed of amorphous nanoblocks deriving from three-dimensional framework $Sb_4O_5Cl_2$ structure, and the surface is composed of irregular nanorods. In particular, nanoblocks and nanorods are not isolated which is attributed to the successful combination of $Sb_2S_3/Sb_4O_5Cl_2$ composites. With a longer reaction time, the brush-like $Sb_2S_3/Sb_4O_5Cl_2$ microcrystallines are gradually organized into unenclosed microspheres via the oriented attachment mechanism[9]. The same irregular nanorods are observed in the interior of microspheres, composed with building units of one-dimensional nanostructure-based blocks and rods. In fact, the three-dimensional framework structure, which is easily formed by the self-assembly of $Sb_4O_5Cl_2$ crystallites at room temperature, is the foundation of synthesizing spherical $Sb_2S_3/Sb_4O_5Cl_2$ composites. Furthermore, three relevant chemical reactions for the synthesis of $Sb_2S_3/Sb_4O_5Cl_2$ hybrid microcrystallines are proposed:

$$4SbCl_3+5H_2O \rightarrow Sb_4O_5Cl_2+10HCl \quad (1)$$

$$6S^{2-}+ Sb_4O_5Cl_2 \rightarrow 2Sb_2S_3+5O^{2-}+2Cl^- \quad (2)$$

$$nSb_2S_3+mSb_4O_5Cl_2 \rightarrow Sb_2S_3/Sb_4O_5Cl_2 \text{ microcrystallines} \quad (3)$$

3.2.4 The effect of hydrochloric acid or NaOH concentration

The idea on the formation mechanism of the three-dimensional framework $Sb_4O_5Cl_2$ structure based on the effect of the concentration of hydrochloric acid or NaOH is established. Accordingly, one contrast experiment is taken in another HCl concentration without adding NaOH, another contrast experiment is taken in the same

HCl concentration without adding NaOH. Fig. S6 presents the general morphologies of the samples synthesized without NaOH, it shows that the samples prepared in different HCl concentration are in the form of microrods, and no spheres can found. However, for the samples prepared in the same HCl concentration, lots of nanorods appear with some olivary spheres (Fig. S6). The results clarify that HCl concentration plays a vital role in the formation of the three-dimensional framework $Sb_4O_5Cl_2$ structure. Three-dimensional $Sb_4O_5Cl_2$ structures are formed under the action of specific concentration of HCl and stirring. Effectively, NaOH is suitable for adjusting the HCl concentration in the mixture solution. Obviously, the morphology samples resulted from the contrast trials are different from C1, C2 and C3 (Fig. S6 and Fig. S3), supposing that NaOH also has generated significant influence on the direction and size of crystal growth during the period of neutralization for sodium hydroxide and hydrochloric acid.

3.3 Mechanisms

On the basis of these experiments, the possible mechanistic pathway in the formation of spherical structures is illustrated in Fig. 3. $Sb_4O_5Cl_2$ nanoparticles form at early stages, and then aggregate into nanoblocks and self-assemble into an abnormal three-dimensional structure. With releasing of S^{2-} from Na_2S, a react with $Sb_4O_5Cl_2$ by ion exchange leads to the combination of $Sb_2S_3/Sb_4O_5Cl_2$ microcrystallines. Finally, with the increase of reaction time, the microcrystallines gradually self-assemble into regular spheres. Besides, since no surfactants or

emulsions are used, the geometrical shape of building units must play a key role in the formation of spherical structure[5].

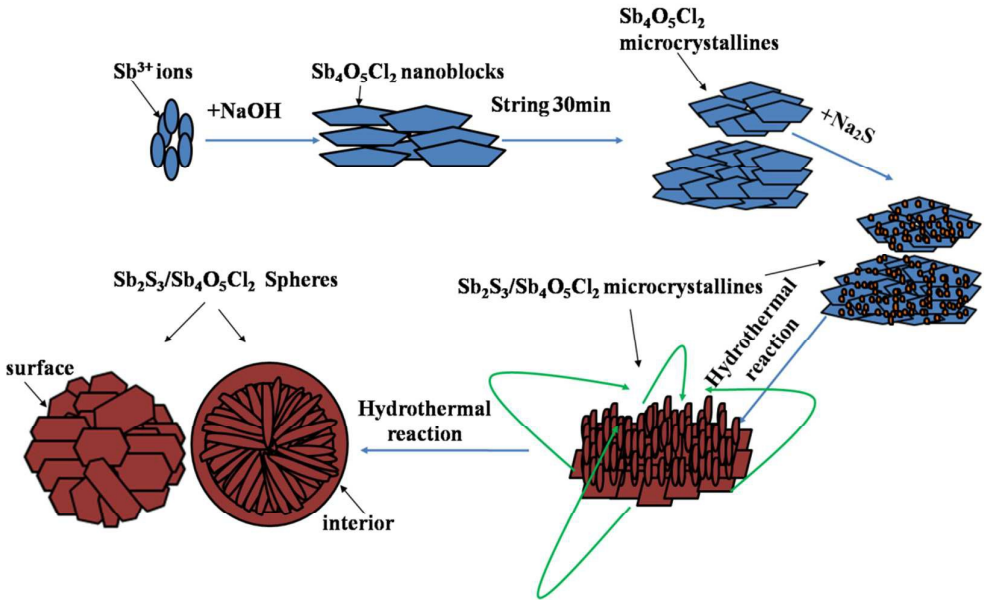

Fig.3. A schematic illustration of the formation of spherical $Sb_2S_3/Sb_4O_5Cl_2$.

3.4 Optical property and photocatalytic activity evaluation

The optical properties of the products are studied by UV-vis reflectance spectroscopy, and the corresponding UV-vis absorption spectrum of $Sb_4O_5Cl_2$, C1, C2 and C3 are shown in Fig. 4a. Compared to the $Sb_4O_5Cl_2$, $Sb_2S_3/Sb_4O_5Cl_2$ composites exhibit a strong absorption in both UV and visible range due to the introduced Sb_2S_3, suggesting that $Sb_2S_3/Sb_4O_5Cl_2$ composites are excited by visible light. It is well-known that the relation between the absorption coefficient and the band gap energy of an indirect-gap semiconductor is described by the formula $(\alpha h\nu)^2 = A(h\nu - Eg)$, Where α, ν, Eg and A are absorption coefficient, light frequency, band gap energy, and a constant, respectively[12]. Then the band gap values of the synthesized samples are calculated: The band gap energies of $Sb_4O_5Cl_2$, C1, C2 and C3 are

estimated to be 3.25, 2.6, 2.45, and 2.83 eV, respectively (Fig. S7). Considering the optical absorption is a noticeable factor of photocatalytic performance, the $Sb_2S_3/Sb_4O_5Cl_2$ hybrids may be used as photocatalyst under visible light irradiation.

Further, the photocatalytic activity of $Sb_2S_3/Sb_4O_5Cl_2$ is evaluated by the degradation of MO, a representative organic dyestuff. Fig. 4b presents the variation of the MO concentration (C/C_0) as a function of the irradiation time over $Sb_2S_3/Sb_4O_5Cl_2$ photocatalysts. The dark experiment with no significant changes means that the adsorption-desorption equilibrium is achieved after 60 min stirring at dark. As a photocatalyst, $Sb_4O_5Cl_2$ shows no photocatalytic activity for the degradation of MO because of its band gap energy. As shown in Fig. 4b, the degradation efficiency of the C1, C2 and C3 are 64.3%, 82.9%, and56.2% after 60 min, indicating that C2 has higher catalytic activity than C1 and C3 under visible light, which is consistent with the results of UV-vis reflectance spectroscopy (Fig. 4a). However, the difference in the photocatalytic activity of different samples is based on many factors, including morphology, specific surface area, optical absorption, band gap, composition, crystallinity, etc. A systematic investigation should be progressed in the future research. Most importantly, this $Sb_2S_3/Sb_4O_5Cl_2$ composite also has great potentiality in the applications of photoelectric conversion and solar cell.

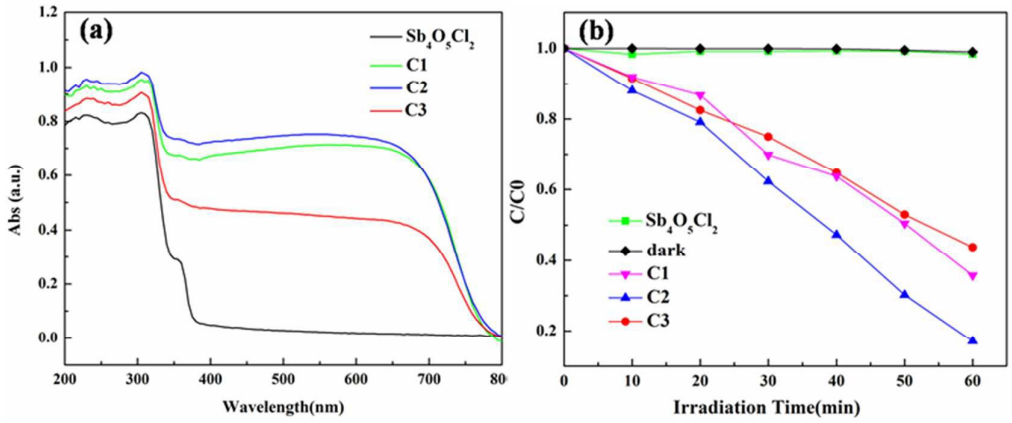

Fig.4. (a) UV–vis diffuse reflectance spectra of different samples; (b) Photocatalytic degradation of MO over different samples under visible light (λ≥420 nm) irradiation.

4. Conclusions

In summary, spherical structure of $Sb_2S_3/Sb_4O_5Cl_2$ composed of nanoblocks was firstly synthesized by a facile hydrothermal route without any surfactants. The mechanism in the combination of $Sb_2S_3/Sb_4O_5Cl_2$ composites is an anion exchange strategy. The suitable temperature and hydrochloric acid concentration played crucial roles in the formation of spherical structures. Furthermore, the band gaps of the products were deduced from UV spectra, the $Sb_2S_3/Sb_4O_5Cl_2$ samples exhibited a suitable bad gap between 2.45 and 2.83 eV, and the photocatalytic efficiency of the as-prepared materials C2 for the degradation of MO can reach 82.9% after 60 min. It is believed that this composite may be the potential optoelectronic material.

Acknowledgments

The authors gratefully acknowledge the financial support provided by Collaborative Innovation Center of Resource–Conserving & Environment-friendly Society and Ecological Civilization, the Hunan Province Innovation Foundation for Postgraduate

(No. CX2014B142), the National Natural Science Foundation of China (No. 71431006).

Reference

1. Y. Cui and C. M. Lieber, *Science*, 2001, **291**, 851-853.

2. G. M. Whitesides and B. Grzybowski, *Science*, 2002, **295**, 2418-2421.

3. P. Yang, *Nature*, 2003, **425**, 243-244.

4. S. Park, J. H. Lim, S. W. Chung and C. A. Mirkin, *Science*, 2004, **303**, 348-351.

5. Q. Han, J. Lu, X. Yang, L. Lu and X. Wang., *Cryst. Growth Des*, 2008, **8**, 395-398.

6. Y. Liu, X. Yuan, H. Wang, X. Chen, S. Gu, Q. Jiang, Z. Wu, L. Jiang and G. Zeng, *RSC Adv.*, 2015, **5**, 33696-33704.

7. X. Yuan, H. Wang, Y. Wu, X. Chen, G. Zeng, L. Leng and C. Zhang, *Catalysis Communications*, 2015, **61**, 62-66.

8. H. Wang, X. Yuan, G. Zeng, Y. Wu, Y. Liu, Q. Jiang and G. Gu, *Adv. Colloid Interface Sci*, 2015, **221**, 41-59.

9. B. Liu and H. C. Zeng, *J. AM. CHEM. SOC*, 2004, **126**, 8124-8125.

10. G. Xu, H. Bai, X. Huang, W. He, L. Li, G. Shen and G. Han, *J. Mater. Chem. A*, 2014, **3**, 547-554.

11. J. Ota, P. Roy, S. K. Srivastava, B. B. Nayak and A. K. Saxena., *Cryst. Growth Des*, 2008, **8**, 2019-2023.

12. J. Chao, B. Liang, X. Hou, Z. Liu, Z. Xie, B. Liu, W. Song, G. Chen, D. Chen and G. Shen, *Optics express*, 2013, **21**, 13639-13647.

13. N. Maiti, S. H. Im, Y. H. Lee and S. I. Seok, *ACS applied materials & interfaces*, 2012, **4**, 4787-4791.

14. B. y. xie, J. Huang, B. Li, Y. Liu and Y. Qian, *Adv Mater*, 2000, **20**, 1523-1526.

15. J. Goldberger, R. He, Y. Zhang, S. Lee, H. Yan, H. J. Choi and P. Yang, *Nature*, 2003, **422**, 599-602.

16. Y. C. Zhang, Z. N. Du, K. W. Li, M. Zhang and D. D. Dionysiou, *ACS applied materials & interfaces*, 2011, **3**, 1528-1537.

17. Y. X. Yu, W. X. Ouyang, Z. T. Liao, B. B. Du and W. D. Zhang, *ACS applied materials & interfaces*, 2014, **6**, 8467-8474.

18. H. Wang, X. Yuan, Y. Wu, X. Chen, L. Leng, G. Zeng. RSC Adv., 2015, **5**, 32531-32535.

19. H. Wang, X. Yuan, Y. Wu, G. Zeng, X. Chen, L. Leng, H. Li. App Catal B: Environ. 2015, **174**, 445–454.

20. M. Y. Lu, J. Song, M. P. Lu, C. Y. Lee, L. J. Chen and Z. L. Wang, *ACS NANO*, 2009, **3**, 357-362.

21. Y. C. Zhang, L. Yao, G. Zhang, D. D. Dionysiou, J. Li and X. Du, *Applied Catalysis B: Environmental*, 2014, **144**, 730-738.

22. H. Cheng, B. Huang, X. Qin, X. Zhang and Y. Dai, *Chemical communications*, 2012, **48**, 97-99.

23. B. Lu and J. Tang, *Dalton transactions*, 2014, **43**, 13948-13956.

24. W. Lou, M. Chen, X. Wang and W. Liu., *ACS Chem. Mater*, 2007, **19**, 872-878.

25. J. A. Chang, S. H. Im, Y. H. Lee, H. J. Kim, C. S. Lim, J. H. Heo and S. I. Seok, *Nano letters*, 2012, **12**, 1863-1867.

26. C. S. Lim, S. H. Im, H. J. Kim, J. A. Chang, Y. H. Lee and S. I. Seok, *Physical chemistry chemical physics : PCCP*, 2012, **14**, 3622-3626.

27. H. Zhang, M. Ge, L. Yang, Z. Zhou, W. Chen, Q. Li and L. Liu, *The Journal of Physical Chemistry C*, 2013, **117**, 10285-10290.

28. J. Zhong, X. Zhang, Y. Zheng, M. Zheng, M. Wen, S. Wu, J. Gao, X. Gao, J. M. Liu and H. Zhao, *ACS applied materials & interfaces*, 2013, **5**, 8345-8350.

29. D. H. Kim, S. J. Lee, M. S. Park, J. K. Kang, J. H. Heo, S. H. Im and S. J. Sung, *Nanoscale*, 2014, **DOI: 10.1039/ C4NR04148H**.

30. M. Sun, D. Li, W. Li, Y. Chen, Z. Chen and a. X. F. Y. He, *J. Phys. Chem. C*, 2008, **112**, 18076-18081.

31. X. B. Cao, L. Gu, L. J. Zhuge, W. J. Gao, W. C. Wang and S. F. Wu, *Advanced Functional Materials*, 2006, **16**, 896-902.

32. Q. Han, Y. Yuan, X. Liu, X. Wu, F. Bei, X. Wang and K. Xu, *Langmuir : the ACS journal of surfaces and colloids*, 2012, **28**, 6726-6730.

33. J. Ota and S. K. Srivastava, *Cryst. Growth Des*, 2007, **7**, 343-347.

34. X. Y. Chen, H. S. Huh and S. W. Lee, *Journal of Solid State Chemistry*, 2008, **181**, 2127-2132.